Optical field profile evaluation on silica high-mesa waveguide for infrared absorption sensing

Hokazono, Hirohito
Department of Applied Science for Electronics and Materials, Kyushu University : Graduate student

Jiang, Haisong
Department of Applied Science for Electronics and Materials, Kyushu University : Assistant Professor

Hamamoto, Kiichi
Department of Applied Science for Electronics and Materials, Kyushu University : Professor

https://doi.org/10.15017/1812436

出版情報：九州大学大学院総合理工学報告. 38 (1), pp.1-6, 2016-09. 九州大学大学院総合理工学府
バージョン：
権利関係：

九州大学大学院総合理工学府報告
第 38 巻 第 1 号 1-6 頁 平成 28 年 9 月

Engineering Sciences Reports, Kyushu University
Vol. 38, No. 1, pp. 1-6, SEP., 2016

Optical field profile evaluation on silica high-mesa waveguide for infrared absorption sensing

Hirohito HOKAZONO *1 Haisong JIANG *2, † and Kiichi HAMAMOTO *2
† E-mail of corresponding author: *jiang@asem.kyushu-u.ac.jp*

(Received June 14, 2016, accepted July 1, 2016)

Breathe sensing system that incorporates waveguide gas cells has been proved to be handy for performing daily breath checks. One critical issue for high-sensitivity breath sensing has been high propagation loss. We previously proposed the utilization of a silica high-mesa waveguide due to its low propagation loss. However, till date, few studies have demonstrated that a certain portion of the propagation light profiles out from the waveguide that contributes to infrared absorption sensing so far. In this study, we provide experimental evidence that a certain portion of the propagation light profiles out on an actually fabricated silica high-mesa waveguide for the first time.

Key words: *Breath sensing, silica high-mesa waveguide, FFP reverse-Fourier transformation method*

1. Introduction

A breath-sensing system incorporating waveguide gas cells has proved to be handy for performing daily breath checks.[1)-3)] One critical issue for high-sensitivity breath sensing has been high propagation loss. For instance, in the case of Si/SiO_2 high-mesa waveguide for which the propagation loss is 0.9 dB/cm (at λ = 1550 nm, w = 0.8 μm), performing high-sensitivity breath sensing is difficult because the propagation loss is higher than the gas absorption[4)-5)]. We previously proposed the use of a silica high-mesa waveguide due to its low propagation loss, illustated in Fig. 1[6)]. The silica high-mesa waveguide comprises GeO_2-doped SiO_2 core and SiO_2 cladding. Relative refractive index difference (Δn) of the waveguide in the perpendicular direction is set as 2.5 %. Low refractive index contrast between air and the core of the waveguide contributes to less suffering from the side-wall roughness, in addition to the low absorption loss inherent to the material. The lateral confinement of the waveguide is realized by the so-called high-mesa structure. Figure 2 shows the optical field of a silica high-mesa waveguide simulated using finite element method (FEM) when the waveguide width is 2.2 μm. As the side-wall of the core directly faces to the outside, a certain portion of optical field propagetes out of the waveguide (here, we define this value as Γ_{out}[7)]), which is utilized for gas absorption[8-9)]. However, not enough experimental evidence exits to confierm the existence of the portion of optical field that propagete out of the waveguide. Such

*1 Department of Applied Science for Electronics and Materials, Graduate student
*2 Department of Applied Science for Electronics and Materials

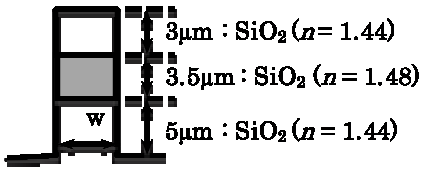

Fig.1 Cross sectional view of silica high-mesa waveguide.

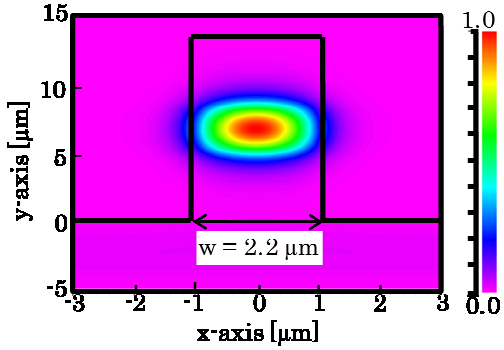

Fig. 2 Optical field of the silica high-mesa waveguide.

a portion of optical field only exists at approximatly 0.2 μm from the waveguide side-wall, as is shown in Fig. 2. Thus, we need to measure the optical field of the waveguide cross section (near field pattern; NFP) with a precision of around 0.01 μm to detect the portion of optical field that propagates out of the waveguide. Performing the NFP measureing method with a precition of 0.01 μm is, however, difficult because it is normally monitored through a lens system that degrades the precision in position. Here, we focus on the relation between NFP and far field pattern (FFP) using Fourier transformation. FFP is the angle component of the optical field propagated from the waveguide facet.

In this study, we demonstrate a method for measuring NFP of optical waveguide by reverse-Fourier transformation of FFP. In addition, the experimental evidence that a certain portion of optical field propagates out of waveguide is obtained by fabricating a silica high-mesa waveguide for infrared absorption spectroscopy. Moreover, it is succesfully confirmed for the first time that 5.8% of the potical field propagetes out of the waveguide.

2. Optical field profile evaluation of NFP by reverse-Fourier transformation of the FFP

2.1 Relation between NFP and FFP

Figure 3 shows that the coordinate system of the Fresnel–Kirchhoff diffraction formula[10]. The waveguide facet is located at $z = 0$. The output of optical field from the waveguide facet propagates to the z-axis direction in free space. When the optical field profile of the NFP is $f(x, y, R)$ and the optcial field profile of the FFP located in $z = R$ is $f(x, y, R)$, the relation between NFP and FFP is obtaind using Fresnel–Kirchhoff diffraction formula as follows:

$$f(x,y,z) = \frac{kn}{j2\pi}\int_{-\infty}^{\infty}\int_{-\infty}^{\infty} f(x_0,y_0,0)\frac{1}{r}\exp(jknr)dx_0dy_0 \quad (1)$$

and

$$r = [(x-x_0)^2 + (y-y_0)^2 + R^2]^{\frac{1}{2}}, \quad (2)$$

where k is the wave number and n is the refractive index in free space. The refractive index is 1 due to propagation of air in free space.

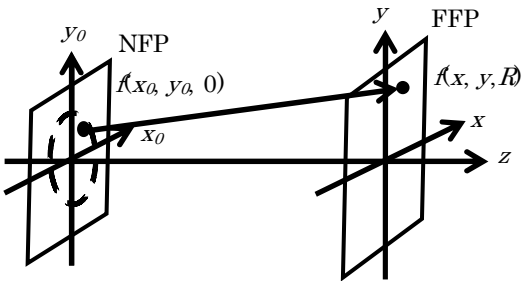

Fig. 3 Coordinate system of Fresnel-Kirchhoff diffraction formula.

Using the approximation of $z >> |x - x_0|$, $|y - y_0|$, equation (2) is rewritten as follows:

$$r = R\left[1 + \frac{(x-x_0)^2+(y-y_0)^2}{R^2}\right]^{\frac{1}{2}} \cong R + \frac{(x-x_0)^2+(y-y_0)^2}{R} + \cdots$$
$$= R + \frac{x^2+y^2}{2R} - \frac{xx_0+yy_0}{R} + \frac{x_0^2+y_0^2}{2R} + \cdots. \quad (3)$$

In Eq. (3), the approximation until the third term is called FFP or the Fraunhoffer region, and the approximation until the fourth term is called the Fresnel region. By approximating Eq. (1) in Fraunhoffer region, the following equation is obtained:

$$f(x,y,z) = \frac{\exp(jkR)}{j\lambda R}\underline{\underline{\exp\left(jk\frac{x^2+y^2}{2R}\right)}} \times \int_{-\infty}^{\infty}\int_{-\infty}^{\infty} f(x_0,y_0,0)\exp\left(-jk\frac{xx_0+yy_0}{R}\right)dx_0dy_0. \quad (4)$$

Thue underlined term in Eq. (4) is ignored because it is constant at the obsrevation point. The double-underlined term that represents the phase delay from the origin to observation point is omitted because this term tends to unity when calculating the optical intensity. Thus, the relation between NFP and FFP is assessed using Fourier transformation.

2.2 Reverse-Fourier transformation of the FFP to NFP

Here, we define the optical field profile of NFP as f_N and the optical field profile of FFP as f_F. In addition, we define $x = R\cos\theta_x$ and $y = R\sin\theta_y$ because FFP is a polar coordinate component. Equation (4) is rewritten as follows:

$$f_F(\theta_x,\theta_y) = \int_{-\infty}^{\infty}\int_{-\infty}^{\infty} f_N(x_0,y_0) \times \exp\{-jk(x_0\sin\theta_x + y_0\sin\theta_y)\}dx_0dy_0. \quad (5)$$

On applying reverse-Fourier transformation, Eq. (5) becomes

$$f_N(x_0,y_0) = \int_{-\infty}^{\infty}\int_{-\infty}^{\infty} f_F(\theta_x,\theta_y) \times \exp\{jk(x_0\sin\theta_x + y_0\sin\theta_y)\}d\theta_xd\theta_y \quad (6)$$

Eq. (6) is not, however, a reverse-Fourier transformation. Asuuming that $\sin\theta_x = \theta_x$ and

$\sin\theta_y = \theta_y$ in case of θ_x, $\theta_y = 0$, Eq. (6) becomes as follows:

$$f_N(x_0, y_0) = \int_{-\infty}^{\infty}\int_{-\infty}^{\infty} f_F(\theta_x, \theta_x) \times \exp\{jk(x_0\theta_x + y_0\theta_y)\}dx_0 dy_0. \quad (7)$$

Equation (7) shows that FFP converts to NFP by using reverse-Fourier transformation. To confirm the reverse-Fourier transformation of the FFP to NFP, we simulate the NFP using FEM and the FFP using beam propagation method (BPM) on the silicon waveguide when wavelength is 1550 nm (Fig. 4). Figure 5 shows the optical field and phase of FFP of the silicon waveguide simulated using BPM. Uisng optical field of Fig. 5, we convert FFP to NFP using Eq. (7). The optical field resulting from the conversion of FFP and the optical field simulated using FEM are shown in Fig. 6. The optical field of NFP of FEM and NFP converted from FFP are appared the difference in vicinity of boundary of core and clad of silicon waveguide (x = ±1.0μm). The optical field of NFP, resulting from the conversion of FFP correspond closely with the optical field of NFP simulated using FEM. The difference arises due to the approximation used in Eq. (7).

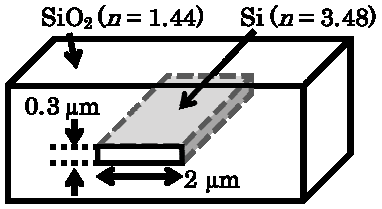

Fig. 4 Schematic of the silicon waveguide.

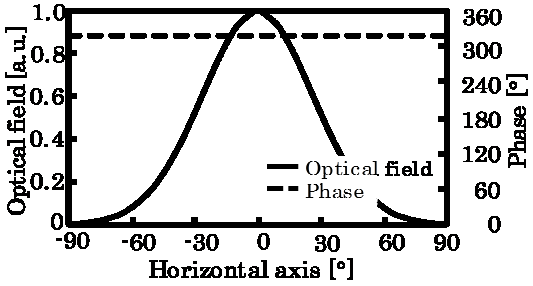

Fig. 5 Optical field and phase of FFP (Fig. 4) simulated using BPM.

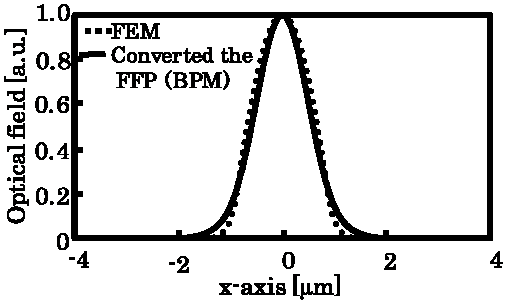

Fig. 6 Optical field of NFP of FEM and converted FFP (Fig. 5).

2.3 Phase of FFP

To convert FFP to NFP, the FFP phase is necessary. However, the result of measuring FFP is not phase profile, as in Fig. 5. Since the phase profile in Fig. 5 is constant (320°), it is possible to assume that the phase profile of FFP is optional phase constant. Figure 7 shows that the result of NFP after using reverse-Fourier transformation that is used the optical field of Fig. 5 and phase profile of 0° constant. In this figure, we confirmed that the optical field of NFP converted from FFP (phase is 0° constant) closely corresponds to the optical field of NFP simulated using FEM.

2.4 The conversion accuracy of reverse-Fourier transformation

In the preceding section, we demonstrated that the optical field of the waveguide facet is obtained using reverse-Fourier transformation of FFP to NFP. Next, we comfirmed the possibility that the conversion accuracy of reverse-Fourier transformation is a function of the silicon waveguide width when the width is changed from 0.4 μm to 5.0 μm. To check the conversion accuracy, we adopted the sample

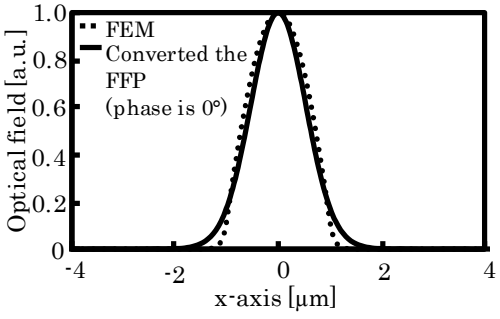

Fig. 7 Optical field of NFP of FEM and converted the FFP (Fig. 4 and phase is 0°).

variance. The sample variance (s^2) is obtained as follows: [11]

$$s^2 = \frac{1}{n-1}\sum_{i=0}^{n}(x_i - X_i)^2 \ , \quad (8)$$

where n is the plot number of optical field, x_i is the optical field of NFP after conversion from FFP, and X_i is the optical field of NFP simulated using FEM. Figure 8 shows the sample variance as a function of the waveguide width obtained using Eq. (8). The sample variance of optical field becomes 0.0015 constant for a waveguide width of 2 μm. Thus, we confirmed that it is possible to convert FFP to NFP for a waveguide width of 2μm with the same accuracy.

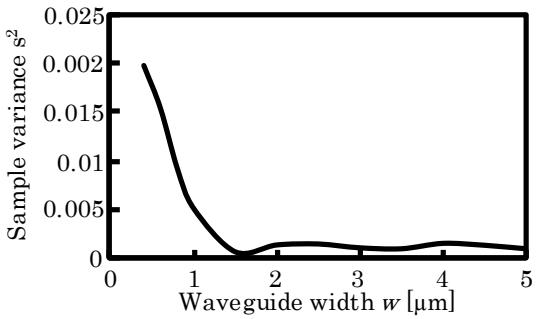

Fig. 8 Sample variance of optical field converting the FFP as a function of waveguide width.

3. The measurement of FFP and conversion to NFP

3.1 Silica high-mesa waveguide

In this section, we explain the fabrication of a silica high-mesa waveguide using measurements of FFP, as is shown in Fig. 1. Figure 2 shows the optical field of the silica high-mesa waveguide simulated by FEM when the waveguide width is 2.2μm and wavelength is 1572nm. We used the wavelenght of 1572 nm as we it is the absorption wavelength of CO_2. As is shown in Fig. 2, a certain portion of optical field exists out of the waveguide. Thus, measuring the gas absorption is possible for applying a certain portion of optical field propagating out of the waveguide. Hence, we confirmed that a certain portion of optical field propagating out of the silica high-mesa waveguide can be measured by reverse-Fourier transformation of FFP.

3.2 Optical field of NFP converted from the FFP of BPM

Figure 9 shows the optical field of Fig. 2 and the conversion of FFP of silica high-mesa waveguide to NFP by reverse-Fourier transformation in the x-axis and the direciotn component in the y-axis (x = 0 μm and y = 6.75 μm). The optical field of NFP simulated using FEM is appeared the discontinuity of optical field in vicinity of boundary of core and air of silica high-mesa waeguide ($x = \pm 1.1$μm), as is shown in Fig. 9(a). The optical field of NFP converted from FFP is a continuous optical field. This difference might be due to the approximation used in Eq. (7). However, we confirmed that the converted FFP of silica high-mesa waveguide corresponds closely to the optical field of NFP simulated using FEM. Moreover, using the optical field converted form FFP, we evaluated the portion of optical field that propagates out of the waveguide.

3.3 Optical field of NFP converted from the measured FFP

Figure 10 shows the experiment design used to measure the FFP of the silica high-mesa waveguide. Three dimensional FFP

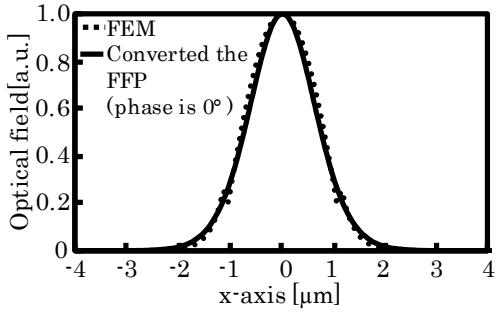

(a) x-axis of NFP

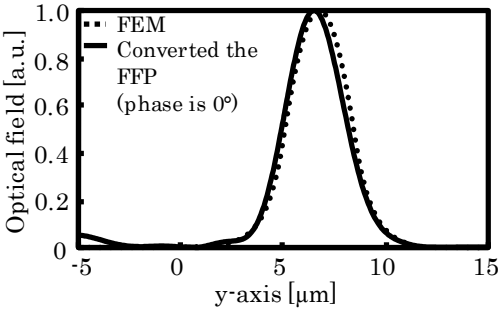

(b) y-axis of NFP

Fig. 9 Optical field of NFP of FEM and converting the FFP of Fig. 8 (phase is 0°).

(wavelength is 1572nm) measurements were obtained via spherical scanning by a photo detector located at the output of the optical field from the silica high-mesa waveguide. Then, we used the LD 8900, which allows real-time measurements of the three-dimensional FFP. Figure 11 shows that the horizontal and vertical direcition components of the optical field of the measured FFP when the waveguide width is 2.2 μm. Figure 12 shows the NFP converted from the measured FFP (Fig. 11), the phase is 0°constant. The optical field of NFP converted from the measured FFP becomes wider than the optical field of NFP obtained using FEM. Because FEM simulates the optical field for the fundamental mode only. The optical field propagating the waveguide includes small high order mode, and high order mode affects both measured FFP and converted NFP. Another possible reason for this could be that the photo detector detects the light that propagates by diffracting from the upper and lower optical waveguide but not the light that simulataneously propagates through the core. However, we experimentally confirmed that a certain portion of optical field propagates out of the silica high-mesa waveguide, as is shown in Fig. 12(a). Thus, silica high-mesa waveguide has the potential to be used for gas sensing by infrared absorption.

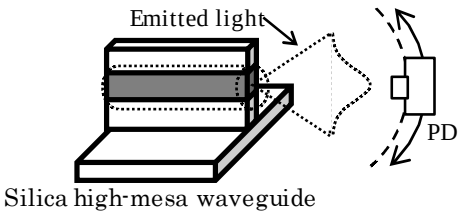

Fig. 10 Experiment design used to measure the FFP of silica high-mesa waveguide.

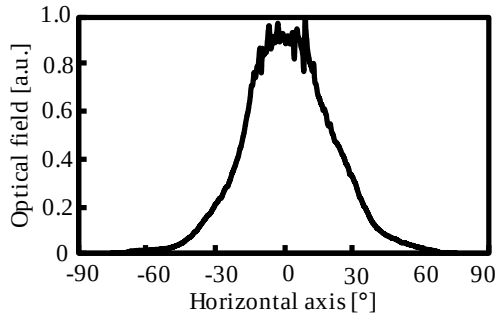

(a) x-axis of FFP

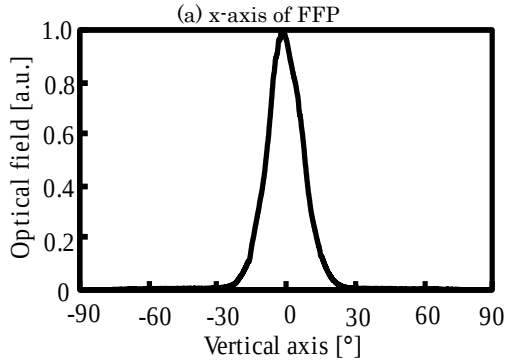

(b) y-axis of FFP

Fig. 11 Optical field of FFP of the silica high-mesa waveguide (waveguide width is 2.2 μm).

4. Evaluation of a certain portion of optical field that propagates out of the waveguide

In the previous section, we confirmed that optical field of NFP converted from measured FFP and FFP obtained using BPM can be measured in case of silica high-mesa waveguide. Using this optical field, we evaluated the portion of optical field that propagates out of the waveguide of silica high-mesa waveguide. The optical field of NFP converted from FFP is

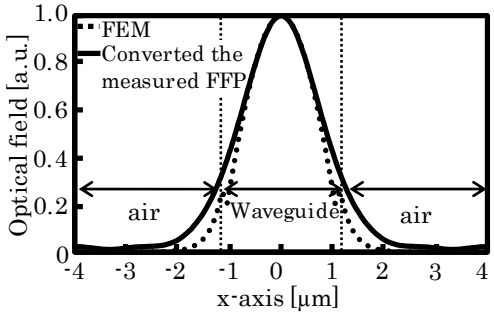

(a) x-axis of NFP

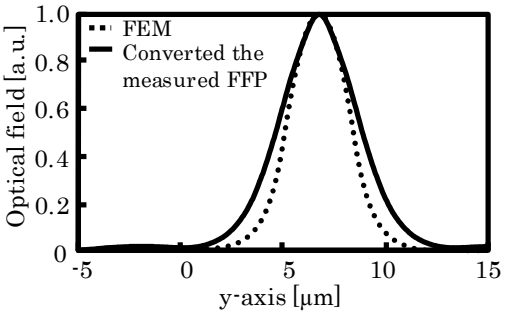

(b) y-axis of NFP

Fig. 12 Optical field of NFP by FEM and converted the measured FFP of silica high-mesa waveguide (waveguide width is 2.2μm).

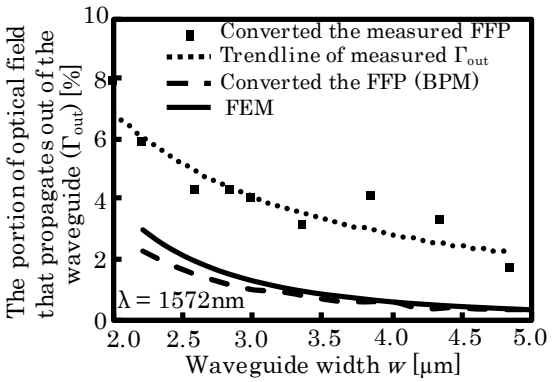

Fig. 13 The portion of optical field that propagates out of the waveguide (Γ_{out}) as a function of waveguide width.

two-dimensional (x- and y-axis direcition components). Thus, we converted the two-dimensional NFP into a three-dimensional NFP. Here, the three-dimensional NFP is $f(x_0,y_0)$; x- and y-axis direcition components are $f_x(x_0)$ and $f_y(y_0)$. We assumed the three-dimensional NFP to follow the equation (9):

$$f(x_0, y_0) = f_x(x_0) f_y(y_0) \quad . \tag{9}$$

Using this eauation (Eq. (9)), we evaluated the portion of optical field that propagates out of the waveguide (Γ_{out}). Figure 13 shows Γ_{out} as a function of waveguide width for the converted FFP and the trendline of the measured Γ_{out}. Converting the FFP obtained using BPM and simulated by FEM. The Γ_{out} of the FFP converted using BPM is only 0.3 % higher than the Γ_{out} simulated using FEM due to the approximation used in Eq. (7). Thus, the assumptions made in Eq. (9) used to convert NFP from two dimensions to three dimensions are valid because the Γ_{out} of both FFPs substantially correspond. Next, we compared the Γ_{out} of converting the measured FFP and the Γ_{out} simulated using FEM. The Γ_{out} of converting the FFP using BPM is 3 % higher that the Γ_{out} simulated by FEM. However, we confirmed that the Γ_{out} of the converted measured FFP decreases with ingcreasing waveguide width. This trend is the same for Γ_{out} simulated using FEM. FEM simulates the optical field for the fundamental mode only. The optical field propagating the waveguide includes small high order mode, and high order mode affects both measured FFP and converted NFP. Furthermore, the photo detector detects the light propagated by diffraction from the upper and lower optical waveguide but not the light that is simultaneously propagated through the core.

5. Conclusions

We have proposed a method to measure NFP of optical waveguide using reverse-Fourier transformation of the FFP. This method provides experimetal evidence that a certain portion of optical field propagates out of the silica high-mesa waveguide for infrared absorption spectroscopy. The results confirm that the method to measure NFP of optical waveguide by reverse-Fourier transformation of the FFP allows for a certain level of accurancy. Moreover, we provide the experimental evidence that 5.8% of optical field propagetes out of the waveguide (for a waveguide width of 2.2μm) on fabricated silica high-mesa waveguide. We concule that the silica high-mesa waveguide has the potential to be used for breath sensing.

References

1) A. Wilk, F. Seichter, S. Kim, E. Tütüncü, B. Mizaikoff, J. A. Vogt, U. Wachter, and P. Radermacher, Anal Bioanal Chem, **402**(1), 397 (2012)
2) S. Kim, C. Young, B. Vidakovic, SGA. Gabram-Mendola, CW, Bayer, and B, Mizaikoff, IEEE Sensors Journal, **10**(1), 145 (2010)
3) W. C. Lai, S. Chakravarty, X. L. Wang, C. Y. Lin, and R. T. Chen, Optics Letters, **36**(6), 984 (2011)
4) J. Workman, "Handbook of organic compounds : NIR, IR, Raman, and UV-Vis spectra featuring polymers and surfactants", San Diego : Academic Press (2001)
5) A. Intekhab, Y. Matsunaga, S. Hirofuji, T. Mitomi, T. Murayama, Y. Kokaze, H. Wado, Y. Takeuchi, and K. Hamamoto, Technical Digest of 15th Microoptics Conference, F3, 90 (2009)
6) J. Chen, H. Hokazono, D. Nakashima, M. Tsujino, Y. Hashizume, M. Itoh, and K. Hamamoto, Japanese Journal of Applied Physics, **53**(2), 022502 (2014)
7) D. Nakashima and K. Hamamoto, Applied Physics Express, **5**(6), 062202 (2012)
8) P. C. Kamat, C. B. Roller, K. Namjou, J. D. Jeffers, A. Faramarzalian, R. Salas, and P. J. McCann, Applied Optics, **46**(19), 3969 (2007)
9) A. O. Wright, and M. B. Frish, Conference on Lasers and Electro-Optics (CLEO), CThII (2007)
10) L.A.Coldren, S.W.Corzine, and M. L. Corzine "Diode Lasers and Photonic Integrated Circuits", Wiley, Appendix 3.4 (1995)
11) H. Sahai and M. I. Ageel, "The analysis of Variance", Springer Science+Business Media, LLC, p. 15 (2000)